Check for updates

How to cite: *Angew. Chem. Int. Ed.* **2025**, *64*, e202509174
doi.org/10.1002/anie.202509174

Crystalline Porous Materials **Hot Paper**

Introducing Functional Groups Into B←N Organic Frameworks with Permanent Porosity

Huifang Zhou, Tiantian Jiang, Kangjian Fu, Xinyu Guan, Shilin Guan, Bo Liu,* and Hai-Long Jiang**

Abstract: Crystalline organic frameworks incorporating dative B←N and reversible B—O bonds (BNOFs) have garnered increasing interest on account of their crystallinity, porosity, and processability. However, strategies for introducing functions into BNOFs remain largely unexplored. In this work, a series of functionalized BNOFs, named BNOF-*n* ($n = 2$–9), have been designed and synthesized using a mixed-monomer assembly strategy. The obtained materials share structural similarities but reveal distinct functional groups, demonstrating excellent chemical stability, high surface areas, and remarkable regenerability. Notably, BNOF-5, functionalized with abundant carboxyl groups, achieves exceptional reversible NH_3 adsorption capacity (up to 10.0 mmol g^{-1} at 1 bar and 298 K), significantly surpassing that of the nonfunctionalized BNOF-1 (5.6 mmol g^{-1}) and the less-functionalized BNOF-7 (7.9 mmol g^{-1}), thereby clearly demonstrating the effectiveness of the functionalization strategy. Remarkably, the damaged BNOF-5 can be efficiently repaired through facile regeneration, highlighting its outstanding recyclability. This work demonstrates the first attempt at functionalization methodology in BNOFs, extending their potential toward diverse applications.

Introduction

Crystalline porous materials (CPMs), characterized by permanent porosity and well-ordered architectures, have garnered significant attention due to their tunable structures and multifunctional properties.[1–5] Among these materials, metal-organic frameworks (MOFs)[6–13] and covalent organic frameworks (COFs)[14–20] stand out as prominent examples, being widely recognized for their atomically precise structures and functional versatility. However, the strong bonding interactions in MOFs and COFs, such as coordination and covalent bonds, typically result in poor solubility and limited processability,[21–23] impeding their regeneration and limiting their practical applications.

In contrast, CPMs constructed via weak supramolecular interactions present a compelling alternative.[24–27] The labile nature of these intermolecular interactions endows these materials with distinct advantages, such as solution processability and regenerability, making them highly attractive for specific applications requiring dynamic reversibility.[28–31] Notably, reversible boron—oxygen (B—O) bonds are widely employed in the construction of supramolecular systems due to their inherent dynamic nature,[32–34] while the additional incorporation of dative boron—nitrogen (B←N) bonds has been shown to synergistically enhance the structural stability without compromising their dynamic behavior.[35,36] Therefore, it is highly desired to construct crystalline organic frameworks incorporating both dative B←N and reversible B—O bonds, denoted as BNOFs.[37–41] It is assumed that these BNOFs not only integrate the processability of supramolecular systems but also possess the well-defined structures as they present similar crystallinity of traditional CPMs.

In recent years, these BNOFs have attracted intensive interest and a growing number of BNOFs have been successfully synthesized.[37–54] However, the absence of permanent porosity in most early examples severely limited their practical utility. Consequently, previous studies have predominantly focused on solution-phase selective separation,[45,46] photosensitivity,[47–49] and mechanical applications.[41,50] Recently, the successful development of BNOFs with permanent porosity has enabled their application in gas separation, such as efficient C_2H_2/CO_2 and hexane isomer separations.[38,39,50,51] Despite this active progress, current investigations on BNOFs remain largely centered on the synthesis of novel framework structures; the efforts toward targeted functionalization are scarce,[52–54] significantly restricting their further applications. To our knowledge,

[*] H. Zhou, T. Jiang, K. Fu, S. Guan, Dr. B. Liu
College of Chemistry & Pharmacy, Northwest A&F University, Yangling 712100, P.R. China
E-mail: chemliubo@nwsuaf.edu.cn

Prof. Dr. H.-L. Jiang
Hefei National Research Center for Physical Sciences at the Microscale, Department of Chemistry, University of Science and Technology of China, Hefei, Anhui 230026, P.R. China
E-mail: jianglab@ustc.edu.cn

Dr. X. Guan
Hangzhou Institute of Advanced Studies, College of Chemistry and Materials Science, Zhejiang Normal University, Hangzhou, Zhejiang 310000, P.R. China
E-mail: guanxy@zjnu.edu.cn

Homepage: http://mof.ustc.edu.cn/

Additional supporting information can be found online in the Supporting Information section

© 2025 Wiley-VCH GmbH

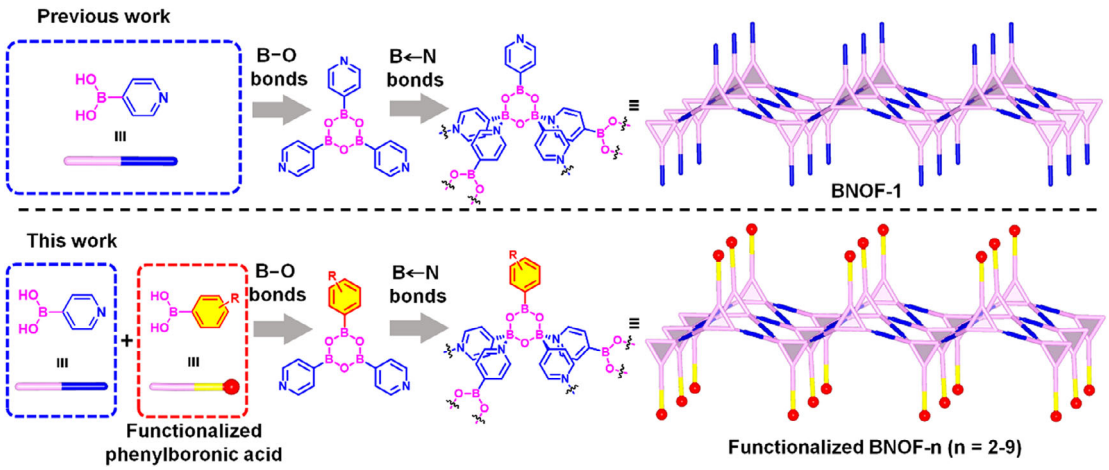

Scheme 1. Schematic illustration showing the synthesis of functionalized BNOFs via the mixed-monomer assembly strategy. Top: BNOF-1 synthesized from the single monomer. Below: Functionalized BNOFs constructed via the mixed-monomer strategy developed in this work, named BNOF-*n* ($n = 2$–9). Functionalized sites are marked with red spheres.

the systematic strategy to tailor their functionality through specific structural modifications in these materials has not yet been reported thus far.

Herein, by adopting the mixed-monomer assembly strategy, a series of BNOFs, named BNOF-*n* ($n = 2$–9), have been synthesized and modified with diverse functional groups (Scheme 1). These functionalized frameworks can be easily prepared at gram scale, exhibiting excellent chemical stability, high surface areas, and remarkable regenerability. Notably, BNOF-5, which incorporates abundant carboxyl groups as functional sites, demonstrates superior reversible NH_3 adsorption through acid–base interactions, achieving a remarkable uptake capacity of 10.0 mmol g^{-1} at 1 bar and 298 K. This performance significantly surpasses those observed for the nonfunctionalized BNOF-1 (5.6 mmol g^{-1}) and less-functionalized BNOF-7 (7.9 mmol g^{-1}) under the identical conditions, unambiguously highlighting the significance of introducing functional groups. Furthermore, the damaged BNOF-5 can be fully restored via simple regeneration, highlighting its exceptional sustainability. To the best of our knowledge, this work represents the first investigation of introducing functional groups into BNOFs, laying a foundation for their tailored application to diverse ends.

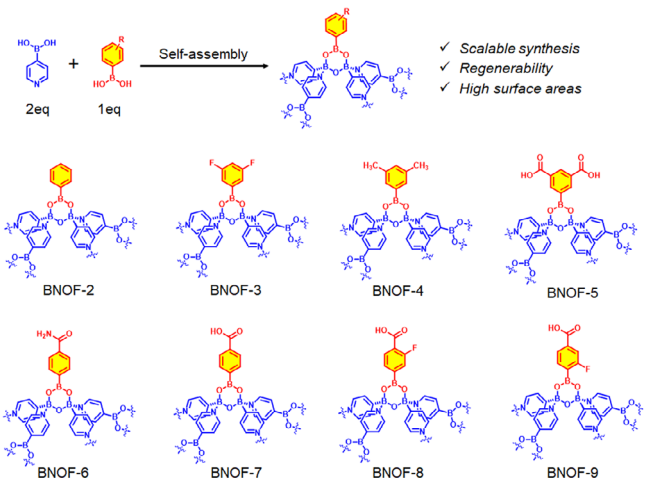

Figure 1. Synthetic route of functionalized BNOFs through copolymerization of pyridine-4-boronic acid and varied functionalized boronic acid monomers with a molar ratio of 2:1.

Results and Discussion

The systematic functionalization strategy is based on the structural insights of the previously reported BNOF-1,[39] in which the pyridine-4-boronic acid (PBA) exhibits dual connection modes: two-thirds of the PBA molecules act as bridging linkers (denoted as PBA_{linker}), leveraging both pyridine and boronic acid moieties to assemble the 2D layers, while the remaining one-third function as terminal units (denoted as $PBA_{terminal}$), dangling solely through boronic acid condensation with the pyridine moieties exposed (Figures 1 and S1). Motivated by the dual roles of PBA in BNOF-1, the other functionalized BNOFs are designed and synthesized by replacing $PBA_{terminal}$ with a series of phenylboronic acid derivatives involving fluorinated, methyl, carboxylic acid, and amide groups (Figure S2). Generally, these monomers are solvothermally reacted with PBA in a mixed solvent system of *N*-methylformamide, MeCN, and formic acid, resulting in the successful formation of single crystals of eight distinct functionalized BNOFs (i.e., BNOF-2–9) (for details, see the Supporting Information).

The crystal structures of BNOFs can be definitively determined through single-crystal X-ray diffraction (XRD) (Table S1). In the structures of BNOF-2–9, the boronic acid groups from two PBA molecules and one functionalized phenylboronic acid are condensed into a boroxine unit, with additional two PBA molecules coordinating to B atoms via dative B←N bonds with the bond lengths ranging from 1.625 to 1.654 Å (Figures 1, S3, and Table S2). As a result,

© 2025 Wiley-VCH GmbH

15213773, 2025, 30, Downloaded from https://onlinelibrary.wiley.com/doi/10.1002/anie.202509174 by University Of Science, Wiley Online Library on [13/08/2025]. See the Terms and Conditions (https://onlinelibrary.wiley.com/terms-and-conditions) on Wiley Online Library for rules of use; OA articles are governed by the applicable Creative Commons License

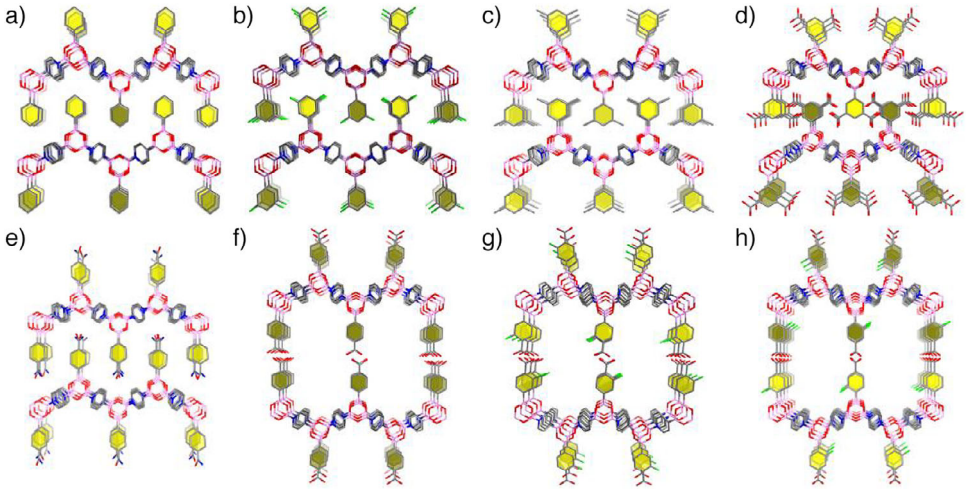

Figure 2. Supramolecular frameworks of a) BNOF-2, b) BNOF-3, c) BNOF-4, d) BNOF-5, e) BNOF-6, f) BNOF-7, g) BNOF-8, and h) BNOF-9 along the *a* axis. C: gray, N: blue, B: pink, O: red, and F: green (H atoms are omitted for clarity). The *N*-methylformamide solvent molecules incorporated in the frameworks exhibit severe disorder and have been subsequently removed using the SQUEEZE/solvent mask procedure.

each boroxine unit connected with four neighboring boroxine units through pyridine bridges, forming a 2D layer with sra topology. The functionalized phenyl groups adopt a staggered arrangement across the upper and lower surfaces of the 2D layer. Furthermore, these layers are stacked together by weak intermolecular interactions to give 3D supramolecular frameworks, with interlayer distances ranging from approximately 4.1 to 5.3 Å (Figures 2 and S4). The distinct space groups of BNOFs have been summarized in Table S1. Notably, all the structures from BNOF-2 to BNOF-9 feature high solvent-accessible volumes (41.2%–66.7%) and square open channels (5.9 Å × 9.1 Å to 9.1 Å × 9.6 Å), providing spatially confined yet accessible domains for guest inclusion while maintaining structural rigidity (Figures S5 and S6).

The phase purity of the as-synthesized BNOF samples is confirmed by powder XRD, with the experimental diffraction patterns well matching the simulations from single-crystal structures (Figure S7). Furthermore, the powder XRD patterns of all BNOFs remain unchanged after immersion in various solvents, demonstrating their exceptional stability (Figure S8). Thermogravimetric analysis (TGA) reveals two distinct thermal regimes, including solvent molecule release below approximately 180 °C and structural integrity retention up to approximately 300 °C, confirming robust thermal stability of the BNOFs (Figure S9).

To evaluate the permanent porosity of the BNOFs, N_2 sorption measurements have been performed at 77 K, which display typical type I behavior (Figure 3), indicating the microporous nature of all BNOFs. Notably, the N_2 adsorption isotherm of BNOF-3 displays a distinct two-step adsorption behavior, implying its flexible nature, which can be confirmed by the altered XRD patterns with increasing temperature in the variable-temperature in situ XRD (Figure S10). Based on Brunauer–Emmett–Teller (BET) model, the BNOFs exhibit high surface areas ranging from 484 to 1388 $m^2\ g^{-1}$, surpassing all previously reported BNOFs with permanent porosity, except for BNOF-1 (Table S3). The relatively lower BET surface area of BNOF-6 is possibly due to steric hindrance

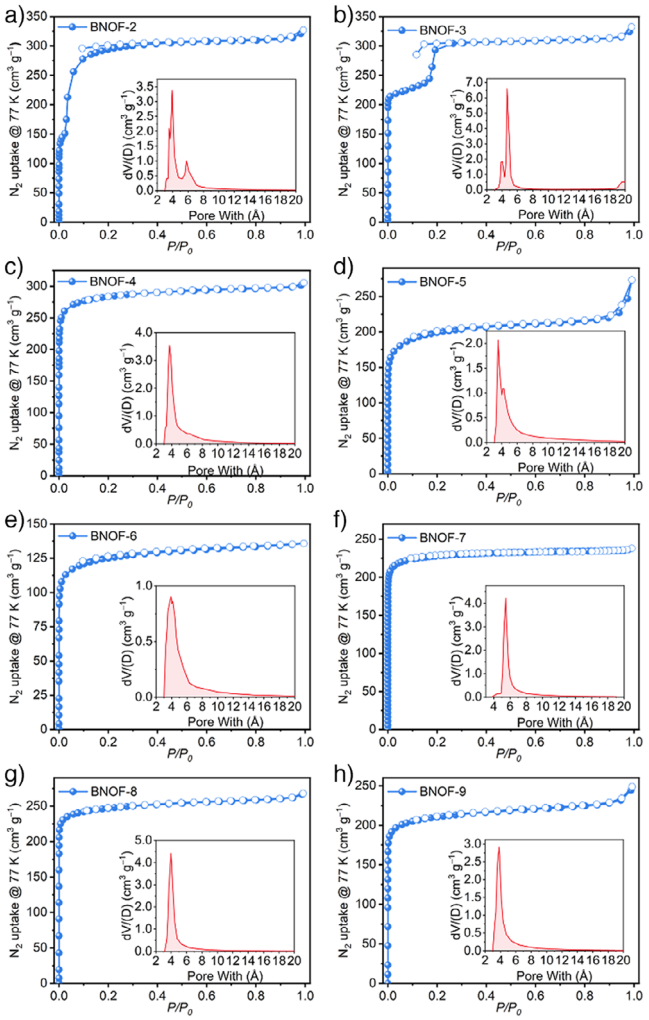

Figure 3. N_2 sorption isotherms and pore size distributions of a) BNOF-2, b) BNOF-3, c) BNOF-4, d) BNOF-5, e) BNOF-6, f) BNOF-7, g) BNOF-8, and h) BNOF-9.

© 2025 Wiley-VCH GmbH

15213773, 2025, 30, Downloaded from https://onlinelibrary.wiley.com/doi/10.1002/anie.202509174 by University Of Science, Wiley Online Library on [13/08/2025]. See the Terms and Conditions (https://onlinelibrary.wiley.com/terms-and-conditions) on Wiley Online Library for rules of use; OA articles are governed by the applicable Creative Commons License

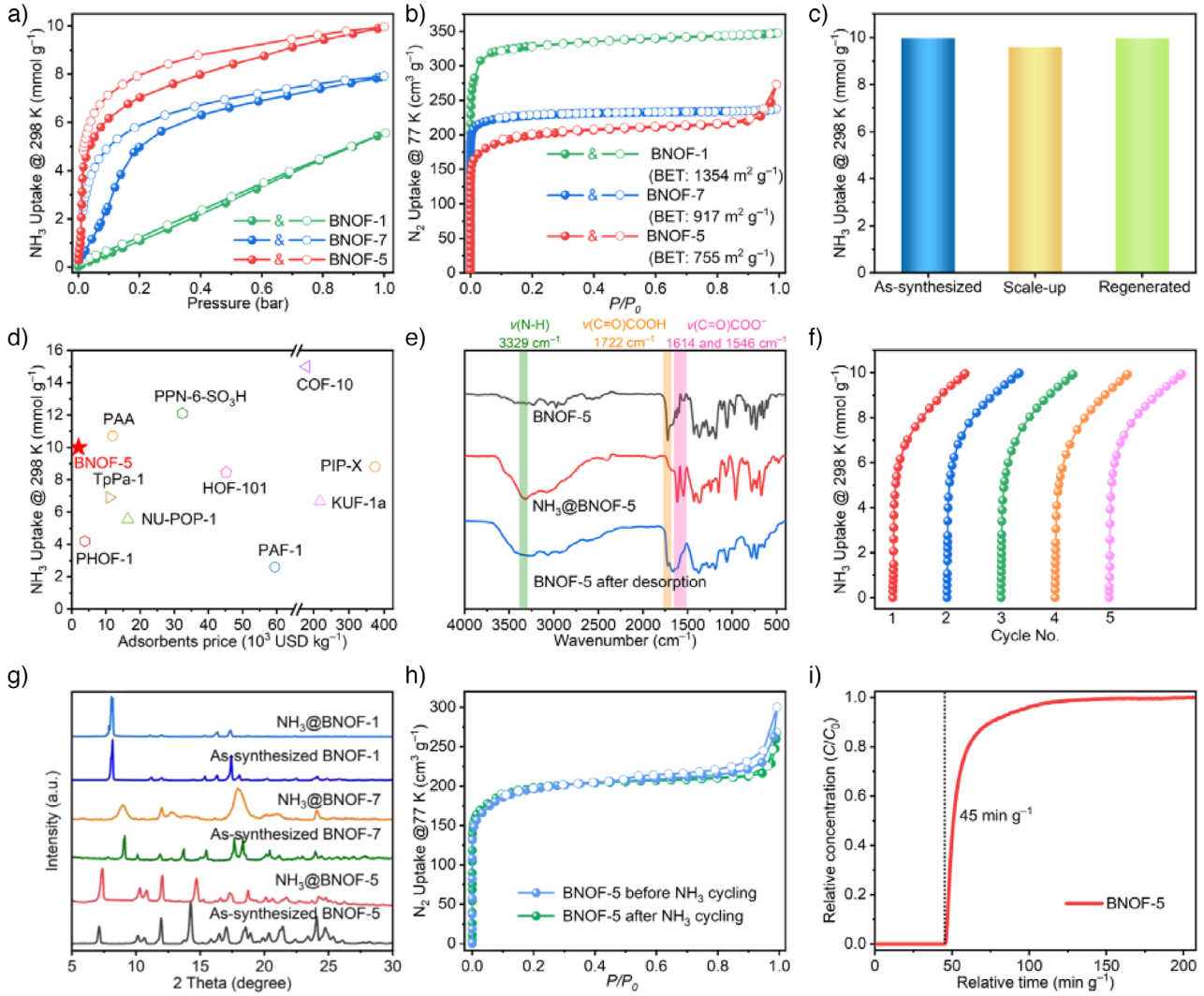

Figure 4. a) NH_3 sorption isotherms of BNOF-1, BNOF-5, and BNOF-7 at 298 K. b) N_2 sorption isotherms of BNOF-1, BNOF-5, and BNOF-7 at 77 K. c) NH_3 adsorption capacities for different samples of BNOF-5 at 298 K and 1 bar. d) Schematic diagram of the cost and NH_3 uptake at 298 K and 1 bar. e) IR spectra of BNOF-5 during NH_3 adsorption–desorption cycles. f) Cyclic NH_3 adsorption capacity of BNOF-5 at 298 K. g) Powder XRD pattern comparison after NH_3 desorption with the as-synthesized one. h) N_2 sorption isotherms of BNOF-5 before and after five NH_3 adsorption–desorption cycles. i) NH_3 breakthrough curve for BNOF-5 in a stream of 0.5% NH_3 and 99.5% N_2 at 298 K with a flow rate of 20 mL min^{-1}.

caused by carbamoylphenyl units, which extend into the pore channels (Figure S5e) and partially limit the diffusion of N_2 molecules. The pore-size distribution (PSD), calculated using the nonlocal density functional theory (NLDFT) model, reveals narrow pore size distributions, which correlate well with the values derived from the crystal structures (Figure 3 (inset) and Table S3). These results indicate the permanent, uniform microporosity of BNOFs, suggesting their potential as candidates for gas storage and separation applications.

The scale-up synthesis, which is crucial for industrial viability, has been further explored for BNOFs. All BNOFs can be easily prepared on a gram scale with high yields (see Experimental Section and Figure S7 in Supporting Information), utilizing commercially available and low-cost monomers. This cost-effective production pathway enables exceptionally low manufacturing costs for BNOFs, especially in comparison to other porous organic materials (Table S4). In addition, these BNOFs can be efficiently resynthesized through facile regeneration process even after structural damage caused by environmental exposure, such as water-induced degradation, as validated by the recovered powder XRD patterns (Figure S11). The combination of regenerability and scalable synthesis, minimizes operational costs, positioning BNOFs as highly promising candidates for practical applications.

As an emerging energy carrier with high energy density, the storage and capture of NH_3 hold great potential for sustainable energy systems.[55,56] Benefiting from the carboxyl-rich channels, high surface area, and excellent chemical stability, BNOF-5 emerges as a promising candidate for NH_3 storage.[57,58] As shown in Figure 4a,b, under ambient conditions (298 K, 1 bar), BNOF-5 achieves a remarkable

© 2025 Wiley-VCH GmbH

15213773, 2025, 30, Downloaded from https://onlinelibrary.wiley.com/doi/10.1002/anie.202509174 by University Of Science, Wiley Online Library on [13/08/2025]. See the Terms and Conditions (https://onlinelibrary.wiley.com/terms-and-conditions) on Wiley Online Library for rules of use; OA articles are governed by the applicable Creative Commons License

NH_3 capacity of 10.0 mmol g^{-1}, significantly surpassing BNOF-1 (5.6 mmol g^{-1}) without carboxylic acid and BNOF-7 (7.9 mmol g^{-1}) with less exposed carboxylic acids, despite the lower BET surface areas of BNOF-5 (755 m^2 g^{-1}) compared with BNOF-1 (1354 m^2 g^{-1}) and BNOF-7 (917 m^2 g^{-1}) (Table S5). These results imply that the significant role of abundant carboxyl groups dangling on the channels toward promoting NH_3 adsorption. Remarkably, the regenerated sample after hydrolyzation also indicates almost unaltered NH_3 capacity (10.0 mmol g^{-1}), demonstrating the durability and reusability of the BNOF-5 framework in NH_3 storage. The BNOF-5 samples synthesized in gram scale can also achieve the high NH_3 uptake of 9.6 mmol g^{-1}, further highlighting their potential for broad-scale application (Figure 4c). This excellent NH_3 uptake performance is comparable to other porous organic materials, including COFs, hydrogen-bonded organic frameworks (HOFs), and porous organic polymers (POPs) (Figure 4d). Notably, BNOF-5 achieves an NH_3 packing density of 0.552 g cm^{-3} at 298 K, approaching the density of liquid NH_3 (0.681 g cm^{-3} at 240 K) (Table S6).[59] Additionally, the slope in the low-pressure region of the NH_3 adsorption isotherm shows a significant upward trend along with the increased carboxylic acid density from BNOF-1 to BNOF-7 to BNOF-5, suggesting the critical role of dangling carboxylic acids in NH_3 capture. The interaction between the carboxylic acid and NH_3 can be further evidenced by FT-IR spectra, with the disappearance of the peak at 1722 cm^{-1} (corresponding to carboxylic acid) and the emergence of new peaks at 1614 and 1546 cm^{-1} (corresponding to the carboxylate) after the NH_3 adsorption (Figure 4e).[56,60] These findings confirm that the abundant carboxylic acid groups in BNOF-5 participate in NH_3 binding, contributing to its superior adsorption performance.

Notably, NH_3 can be efficiently removed from BNOF-5 through simple vacuum treatment at 80 °C, with >99% retention of its original adsorption capacity observed over five consecutive cycles (Figure 4f). FT-IR spectra further demonstrate the close to complete removal of NH_3 after the five cycles, as evidenced by the presence of COOH peak at 1722 cm^{-1} and diminishing of COO^- bands at 1614 and 1546 cm^{-1} (Figure 4e). Additionally, the powder XRD patterns and N_2 sorption isotherms at 77 K display no discernible change after five cycles, indicating the well-preserved crystallinity and porosity throughout the adsorption- desorption process (Figures 4g,h and S12-S14). Dynamic breakthrough tests under a 5000 ppm NH_3 stream reveal strong NH_3 retention for up to 45 min g^{-1} (Figure 4i), validating their practical viability for continuous flow systems. These features of high adsorption capacities, facile preparation, and excellent reusability will position BNOF-5 as a highly promising material for industrial production and applications.

Conclusion

In conclusion, a series of functionalized BNOFs (BNOF-2–9) have been successfully synthesized using a mixed monomer assembly strategy, inspired by the unique structure of BNOF-1. These materials combine excellent chemical stability, high BET surface areas, and remarkable regenerability, making them highly suitable for practical applications. Notably, BNOF-5 decorated with abundant dangling carboxyl groups demonstrates superior reversible NH_3 adsorption reaching up to 10.0 mmol g^{-1} at 1 bar and 298 K, which is significantly higher than that of the nonfunctionalized BNOF-1 (5.6 mmol g^{-1}) and the less-functionalized BNOF-7 (7.9 mmol g^{-1}), underscoring the significance of such a functionalization strategy. Furthermore, BNOF-5 exhibits exceptional sustainability, as it can be easily repaired via regeneration, emphasizing its long-term usability. To the best of our knowledge, this work represents the first systematic exploration of functionalization strategies in BNOFs, providing valuable insights into the design of sustainable and functionalized crystalline organic frameworks toward a wide range of applications.

Acknowledgements

This work was supported by the National Key Research and Development Program of China (2021YFA1500400), the National Natural Science Foundation of China (22331009, U22A20401, and 22205224), the Shaanxi Fundamental Science Research Project for Chemistry & Biology (22JHQ027 and 22JHQ074), and the Natural Science Foundation of Shaanxi Province (2024JC-YBMS-078).

Conflict of Interests

The authors declare no conflict of interest.

Data Availability Statement

The data that support the findings of this study are available from the corresponding author upon reasonable request.

Keywords: B←N organic framework · Crystalline porous materials · Functionalization · Gas adsorption · Microporous materials

[1] H. Li, M. Eddaoudi, M. O'Keeffe, O. M. Yaghi, *Nature* **1999**, *402*, 276–279.
[2] S. Kitagawa, R. Kitaura, S.-i. Noro, *Angew. Chem. Int. Ed.* **2004**, *43*, 2334–2375.
[3] J.-P. Zhang, Y.-B. Zhang, J.-B. Lin, X.-M. Chen, *Chem. Rev.* **2012**, *112*, 1001–1033.
[4] M. O'Shaughnessy, J. Glover, R. Hafizi, M. Barhi, R. Clowes, S. Y. Chong, S. P. Argent, G. M. Day, A. I. Cooper, *Nature* **2024**, *630*, 102–108.
[5] Y. Wu, M. Tang, M. L. Barsoum, Z. Chen, F. Huang, *Chem. Soc. Rev.* **2025**, *54*, 2906–2947.
[6] H. Furukawa, K. E. Cordova, M. O'Keeffe, O. M. Yaghi, *Science* **2013**, *341*, 1230444.
[7] B. Li, H.-M. Wen, Y. Cui, W. Zhou, G. Qian, B. Chen, *Adv. Mater.* **2016**, *28*, 8819–8860.

© 2025 Wiley-VCH GmbH

15213773, 2025, 30, Downloaded from https://onlinelibrary.wiley.com/doi/10.1002/anie.202509174 by University Of Science, Wiley Online Library on [13/08/2025]. See the Terms and Conditions (https://onlinelibrary.wiley.com/terms-and-conditions) on Wiley Online Library for rules of use; OA articles are governed by the applicable Creative Commons License

[8] S. Yuan, L. Feng, K. Wang, J. Pang, M. Bosch, C. Lollar, Y. Sun, J. Qin, X. Yang, P. Zhang, Q. Wang, L. Zou, Y. Zhang, L. Zhang, Y. Fang, J. Li, H.-C. Zhou, *Adv. Mater.* **2018**, *30*, 1704303.
[9] Z. Chen, S. L. Hanna, L. R. Redfern, D. Alezi, T. Islamoglu, O. K. Farha, *Coord. Chem. Rev.* **2019**, *386*, 32–49.
[10] H. Jiang, D. Alezi, M. Eddaoudi, *Nat. Rev. Mater.* **2021**, *6*, 466–487.
[11] G. Wei, Z. Chen, J. Dong, Y. Liu, Y. Cui, *Chem. Rev.* **2022**, *122*, 9078–9144.
[12] W. Wang, Y. Chen, P. Feng, X. Bu, *Adv. Mater.* **2024**, *36*, 2403834.
[13] Q. Yin, Z.-Y. Wang, Z.-B. Fang, H.-X. Liu, Y. Hou, C. Liu, W. Deng, T.-F. Liu, *CCS Chem.* **2024**, https://doi.org/10.31635/ccschem.024.202404630.
[14] C. S. Diercks, O. M. Yaghi, *Science* **2017**, *355*, eaal1585.
[15] K. Geng, T. He, R. Liu, S. Dalapati, K.-T. Tan, Z. Li, S. Tao, Y. Gong, Q. Jiang, D. Jiang, *Chem. Rev.* **2020**, *120*, 8814–8933.
[16] J. Han, J. Feng, J. Kang, J.-M. Chen, X.-Y. Du, S.-Y. Ding, L. Liang, W. Wang, *Science* **2024**, *383*, 1014–1019.
[17] H. Zhuang, C. Guo, J. Huang, L. Wang, Z. Zheng, H.-N. Wang, Y. Chen, Y.-Q. Lan, *Angew. Chem. Int. Ed.* **2024**, *63*, e202404941.
[18] Y. Yin, Y. Zhang, X. Zhou, B. Gui, W. Wang, W. Jiang, Y.-B. Zhang, J. Sun, C. Wang, *Science* **2024**, *386*, 693–696.
[19] F. Chen, H. Zheng, Y. Yusran, H. Li, S. Qiu, Q. Fang, *Chem. Soc. Rev.* **2025**, *54*, 484–514.
[20] K. Wang, X. Qiao, H. Ren, Y. Chen, Z. Zhang, *J. Am. Chem. Soc.* **2025**, *147*, 8063–8082.
[21] J. Jiang, Y. Zhao, O. M. Yaghi, *J. Am. Chem. Soc.* **2016**, *138*, 3255–3265.
[22] L. Hashemi, M. Y. Masoomi, H. Garcia, *Coord. Chem. Rev.* **2022**, *472*, 214776.
[23] L. Geng, Y. Qiao, R. Sun, L. Guo, Z.-Q. Li, Y. Ma, M.-H. Yu, Z. Chang, X.-H. Bu, *Adv. Mater.* **2025**, *37*, 2415511.
[24] R.-B. Lin, Y. He, P. Li, H. Wang, W. Zhou, B. Chen, *Chem. Soc. Rev.* **2019**, *48*, 1362–1389.
[25] Z.-J. Lin, S. A. R. Mahammed, T.-F. Liu, R. Cao, *ACS Cent. Sci.* **2022**, *8*, 1589–1608.
[26] Y. Zou, H.-X. Liu, L. Cai, Y.-H. Li, J.-S. Hu, C. Liu, T.-F. Liu, *Adv. Mater.* **2024**, *36*, 2406026.
[27] X. Meng, S. Zou, J. Li, C. Chen, J. Zhang, M. Wu, *Angew. Chem. Int. Ed.* **2025**, *64*, e202415346.
[28] B.-T. Liu, S.-H. Gong, X.-T. Jiang, Y. Zhang, R. Wang, Z. Chen, S. Zhang, K. O. Kirlikovali, T.-F. Liu, O. K. Farha, R. Cao, *Nat. Synth.* **2023**, *2*, 873–879.
[29] X. Song, Y. Wang, C. Wang, X. Gao, Y. Zhou, B. Chen, P. Li, *J. Am. Chem. Soc.* **2024**, *146*, 627–634.
[30] B. Liu, P. Guo, X. Guan, X. Tian, F. Du, W. Xie, H.-L. Jiang, *Angew. Chem. Int. Ed.* **2024**, *63*, e202405027.
[31] W. Liu, S.-D. Jiang, Y. Yan, W. Wang, J. Li, K. Leng, S. Japip, J. Liu, H. Xu, Y. Liu, I.-H. Park, Y. Bao, W. Yu, M. D. Guiver, S. Zhang, K. P. Loh, *Nat. Commun.* **2020**, *11*, 1633.
[32] C. Gropp, T. Ma, N. Hanikel, O. M. Yaghi, *Science* **2020**, *370*, eabd6406.
[33] M. D. Preuss, T. Schnitzer, S. A. H. Jansen, S. C. J. Meskers, T. H. R. Kuster, X. Lou, E. W. Meijer, G. Vantomme, *Angew. Chem. Int. Ed.* **2024**, *63*, e202402644.
[34] M. Qiao, Y. Li, Y. Li, M. Chang, X. Zhang, S. Yuan, *Angew. Chem. Int. Ed.* **2024**, *63*, e202409951.
[35] Z.-H. Zhao, C.-H. Li, J.-L. Zuo, *SmartMat* **2023**, *4*, e1187.
[36] B. Chen, F. Jäkle, *Angew. Chem. Int. Ed.* **2024**, *63*, e202313379.
[37] E. Sheepwash, V. Krampl, R. Scopelliti, O. Sereda, A. Neels, K. Severin, *Angew. Chem. Int. Ed.* **2011**, *50*, 3034–3037.
[38] H. Zhang, Y. Li, L. Chen, Y. Yang, H. Lin, S. Xiang, B. Chen, Z. Zhang, *Chem* **2023**, *9*, 242–252.
[39] W. Wang, L. Wang, F. Du, G.-D. Wang, L. Hou, Z. Zhu, B. Liu, Y.-Y. Wang, *Chem. Sci.* **2023**, *14*, 533–539.
[40] Q. Dong, T. Naren, L. Zhang, W. Jiang, M. Xue, X. Wang, L. Chen, C.-S. Lee, Q. Zhang, *Angew. Chem. Int. Ed.* **2024**, *63*, e202405426.
[41] D. Xiao, Z. Jin, G. Sheng, L. Chen, X. Xiao, T. Shan, J. Wang, R. Navik, J. Xu, L. Zhou, Q.-H. Guo, G. Li, Y. Zhu, J. F. Stoddart, F. Huang, *Nat. Chem.* **2024**, *16*, 1906–1914.
[42] J. Cruz-Huerta, D. Salazar-Mendoza, J. Hernández-Paredes, I. F. H. Ahuactzic, H. Höpfl, *Chem. Commun.* **2012**, *48*, 4241.
[43] N. Luisier, K. Bally, R. Scopelliti, F. T. Fadaei, K. Schenk, P. Pattison, E. Solari, K. Severin, *Cryst. Growth Des.* **2016**, *16*, 6600–6604.
[44] A. J. Stephens, R. Scopelliti, F. F. Tirani, E. Solari, K. Severin, *ACS Mater. Lett.* **2019**, *1*, 3–7.
[45] X. Wang, Z. Ke, L. Liu, J. Huang, Y. Yang, W. Dai, C. Liu, Z. Zhang, Z. Yao, S. Xiang, *Cryst. Growth Des.* **2021**, *21*, 3168–3174.
[46] C.-H. Liu, L. Chen, H. Zhang, Y. Li, H. Lin, L. Li, J. Wu, C. Liu, Z.-M. Ye, S. Xiang, B. Chen, Z. Zhang, *Chem* **2023**, *9*, 3532–3543.
[47] S. Bhandary, M. Beliš, R. Shukla, L. Bourda, A. M. Kaczmarek, K. V. Hecke, *J. Am. Chem. Soc.* **2024**, *146*, 8659–8667.
[48] J. Xu, T. Wang, S. Deng, W. Lai, Y. Shi, Y. Zhao, F. Huang, P. Wei, *Angew. Chem. Int. Ed.* **2024**, *63*, e202411880.
[49] X. Wang, L. Zhang, X. Wang, T. Cheng, M. Xue, Q. Dong, Y. Peng, Q. Zhang, *Adv. Funct. Mater.* **2024**, *35*, 2401362.
[50] X. Sheng, Z. Wang, G. Sheng, C. Zhu, D. Xiao, T. Shan, X. Xiao, M. Liu, G. Li, Y. Zhu, J. L. Sessler, F. Huang, *J. Am. Chem. Soc.* **2024**, *146*, 12547–12555.
[51] H. Lin, H. Zhang, Y. Li, F. Yuan, X. Zheng, L. He, L. Li, Y. Zhang, S. Xiang, B. Chen, Z. Zhang, *Angew. Chem. Int. Ed.* **2025**, *64*, e202415968.
[52] L. Zhang, Z. Chen, X.-X. Li, X. Wang, Q. Gu, X. Wang, C. S. Lee, Y.-Q. Lan, Q. Zhang, *Angew. Chem. Int. Ed.* **2024**, *63*, e202411018.
[53] Y. Li, H. Chen, J. Huang, H. Zhang, S. Lin, Z.-M. Ye, S. Xiang, B. Chen, Z. Zhang, *J. Am. Chem. Soc.* **2024**, *146*, 19425–19433.
[54] F. Yuan, G. Han, C. Chen, X. Fan, S. Xiang, Z. Zhang, *Angew. Chem. Int. Ed.* **2025**, *64*, e202501875.
[55] R. F. Service, *Science* **2018**, *361*, 120–123.
[56] M. Aziz, A. T. Wijayanta, A. B. D. Nandiyanto, *Energies* **2020**, *13*, 3062.
[57] J. F. Van Humbeck, T. M. McDonald, X. Jing, B. M. Wiers, G. Zhu, J. R. Long, *J. Am. Chem. Soc.* **2014**, *136*, 2432–2440.
[58] K. Ono, T. Ishikawa, S. Masano, H. Kawai, K. Goto, *J. Am. Chem. Soc.* **2024**, *146*, 21417–21427.
[59] C. Marsh, X. Han, J. Li, Z. Lu, S. P. Argent, I. da Silva, Y. Cheng, L. L. Daemen, A. J. Ramirez-Cuesta, S. P. Thompson, A. J. Blake, S. Yang, M. Schröder, *J. Am. Chem. Soc.* **2021**, *143*, 6586–6592.
[60] D. W. Kim, D. W. Kang, M. Kang, D. S. Choi, H. Yun, S. Y. Kim, S. M. Lee, J.-H. Lee, C. S. Hong, *J. Am. Chem. Soc.* **2022**, *144*, 9672–9683.

Manuscript received: April 25, 2025
Revised manuscript received: May 19, 2025
Accepted manuscript online: May 20, 2025
Version of record online: May 27, 2025

© 2025 Wiley-VCH GmbH

15213773, 2025, 30, Downloaded from https://onlinelibrary.wiley.com/doi/10.1002/anie.202509174 by University Of Science, Wiley Online Library on [13/08/2025]. See the Terms and Conditions (https://onlinelibrary.wiley.com/terms-and-conditions) on Wiley Online Library for rules of use; OA articles are governed by the applicable Creative Commons License